THE JOURNAL OF BIOLOGICAL CHEMISTRY VOL. 283, NO. 36, pp. 24922–24934, September 5, 2008

A Conformationally Mobile Cysteine Residue (Cys-561) Modulates Na^+ and H^+ Activation of Human CNT3*[S]

Received for publication, March 5, 2008, and in revised form, July 7, 2008 Published, JBC Papers in Press, July 11, 2008, DOI 10.1074/jbc.M801793200

Melissa D. Slugoski[‡1], Kyla M. Smith[‡], Ras Mulinta[‡], Amy M. L. Ng[‡], Sylvia Y. M. Yao[‡], Ellen L. Morrison[‡], Queenie O. T. Lee[‡], Jing Zhang[§¶], Edward Karpinski[‡], Carol E. Cass[§¶2], Stephen A. Baldwin[‖], and James D. Young[‡3]

From the Membrane Protein Research Group, Departments of [‡]Physiology and [§]Oncology, University of Alberta, Edmonton, Alberta, T6G 2H7, and the [¶]Cross Cancer Institute, Edmonton, Alberta T6G 1Z2, Canada, and the [‖]Astbury Centre for Structural Molecular Biology, Institute of Membrane and Systems Biology, University of Leeds, Leeds LS2 9JT, United Kingdom

In humans, the SLC28 concentrative nucleoside transporter (CNT) protein family is represented by three Na^+-coupled members; human CNT1 (hCNT1) and hCNT2 are pyrimidine and purine nucleoside-selective, respectively, whereas hCNT3 transports both purine and pyrimidine nucleosides and nucleoside drugs. Belonging to a phylogenetic CNT subfamily distinct from hCNT1/2, hCNT3 also mediates H^+/nucleoside cotransport. Using heterologous expression in *Xenopus* oocytes, we have characterized a cysteineless version of hCNT3 (hCNT3C−). Processed normally to the cell surface, hCNT3C− exhibited hCNT3-like transport properties, but displayed a decrease in apparent affinity specific for Na^+ and not H^+. Site-directed mutagenesis experiments in wild-type and hCNT3C− backgrounds identified intramembranous Cys-561 as the residue responsible for this altered Na^+-binding phenotype. Alanine at this position restored Na^+ binding affinity, whereas substitution with larger neutral amino acids (threonine, valine, and isoleucine) abolished hCNT3 H^+-dependent nucleoside transport activity. Independent of these findings, we have established that Cys-561 is located in a mobile region of the hCNT3 translocation pore adjacent to the nucleoside binding pocket and that access of *p*-chloromercuribenzene sulfonate to this residue reports a specific H^+-induced conformational state of the protein (Slugoski, M. D., Ng, A. M. L., Yao, S. Y. M., Smith, K. M., Lin, C. C., Zhang, J., Karpinski, E., Cass, C. E., Baldwin, S. A., and Young, J. D. (2008) *J. Biol. Chem.* 283, 8496–8507). The present investigation validates hCNT3C− as a template for substituted cysteine accessibility method studies of CNTs and reveals a pivotal functional role for Cys-561 in Na^+- as well as H^+-coupled modes of hCNT3 nucleoside transport.

Nucleosides and nucleoside analogs with antineoplastic and/or antiviral activity require specialized nucleoside transporter (NT)[4] proteins for uptake into or release from cells (1–3). NT-mediated transport is therefore a critical determinant of nucleoside and nucleotide metabolism and the pharmacologic actions of nucleoside drugs (3–5). NTs also regulate adenosine availability to cell surface purinoreceptors and profoundly affect neurotransmission, vascular tone, and other physiological processes (5, 6). NTs in human and other mammalian cells belong to two structurally unrelated families of integral membrane proteins: the SLC28 concentrative nucleoside transporter (CNT) family and the SLC29 equilibrative nucleoside transporter (ENT) family (3, 6–8). ENTs are ubiquitously expressed in most, possibly all, cell types, whereas CNTs are found predominantly in intestinal and renal epithelial and other specialized cells (1–4, 6–11).

In humans, the SLC28 protein family is represented by three members. hCNT1 and hCNT2 are pyrimidine nucleoside-selective and purine nucleoside-selective, respectively, whereas hCNT3 transports both pyrimidine and purine nucleosides (12–15). hCNT1 and hCNT2 are predominantly Na^+-coupled cotransporters and share a common Na^+/nucleoside stoichiometry of 1:1 (16–18). hCNT3, in contrast, can utilize electrochemical gradients of Na^+ and/or H^+ to accumulate nucleosides within cells with Na^+/nucleoside and H^+/nucleoside coupling stochiometries of 2:1 and 1:1, respectively (16–19). hCNT3 has a broader tissue and cellular distribution than hCNT1/2 (14) and is especially prominent in kidney (10, 11). Nonmammalian members of the CNT protein family that have been characterized include hfCNT from the ancient marine prevertebrate the Pacific hagfish *Eptatretus stouti* (19), CaCNT from the pathogenic yeast *Candida albicans* (20, 21), CeCNT3 from the nematode *Caenorhabditis elegans* (22), and NupC from the bacterium *Escherichia coli* (23, 24). hfCNT is predominantly Na^+-coupled and, similar to hCNT3, exhibits a Na^+/nucleoside stoichiometry of 2:1 (19). CaCNT, CeCNT3, and NupC function exclusively as H^+/nucleoside

* This work was supported in part by the National Cancer Institute of Canada, with funds from the Canadian Cancer Society and the Alberta Cancer Board. The costs of publication of this article were defrayed in part by the payment of page charges. This article must therefore be hereby marked "*advertisement*" in accordance with 18 U.S.C. Section 1734 solely to indicate this fact.

[S] The on-line version of this article (available at http://www.jbc.org) contains supplemental Figs. S1–S3.

[1] Supported by a Studentship from the Alberta Heritage Foundation for Medical Research.

[2] Canada Research Chair in Oncology.

[3] Heritage Scientist of the Alberta Heritage Foundation for Medical Research. To whom correspondence should be addressed: Dept. of Physiology, 7-55 Medical Sciences Bldg., University of Alberta, Edmonton, Alberta T6G 2H7, Canada. Tel.: 780-492-5895; Fax: 780-492-7566; E-mail: james.young@ualberta.ca.

[4] The abbreviations used are: NT, nucleoside transporter; CNT, concentrative nucleoside transporter; ENT, equilibrative nucleoside transporter; hCNT1, -2, and -3, human CNT1, -2, and -3, respectively; TM, putative transmembrane helix; SCAM, substituted cysteine accessibility method; PCMBS, *p*-chloromercuribenzene sulfonate; MES, 2-(*N*-morpholino)ethanesulfonic acid; sulfo-NHS-LC-biotin, sulfosuccinimidyl-6-(biotinamido) hexanoate.

cotransporters (20, 22, 24). The H^+/nucleoside coupling ratio for CaCNT is 1:1 (20).

Human and other eukaryote CNTs have 13 (or possibly 15) transmembrane helices (TMs), with the C-terminal halves of the proteins showing greatest sequence similarity (14, 25). Prokaryote CNTs lack the first three TMs of their eukaryote counterparts, and functional expression of N-terminally truncated hCNT1/rCNT1 in *Xenopus* oocytes has established that these TMs are not necessary for Na^+-dependent uridine transport activity (25). Consistent with this, chimeric studies involving hCNT1/2 (26), hCNT1/3 (17), and hCNT1/hfCNT (19) have established that residues involved in nucleoside selectivity and Na^+ and H^+ coupling reside in the C-terminal half of the proteins. Mutagenesis studies also reveal a key role for the C-terminal residues. In hCNT1, for example, two sets of adjacent residues in TMs 7 and 8 have been identified (Ser^{319}/Gln^{320} and Ser^{353}/Leu^{354}) that, when converted to the corresponding residues in hCNT2, change the nucleoside specificity from CNT1 type to CNT2 type (26). Confirming the roles of these residues in hCNT1/2 nucleoside selectivity, the double TM 8 mutant (S353T/L354V) exhibits a unique uridine-preferring transport phenotype (27). Mutation of Leu^{354} alone markedly increased the affinity of the transporter for Na^+ and Li^+ (27). Also in hCNT1, Glu^{308} and Glu^{322} in TM 7 and Glu^{498} in the region between TMs 11 and 12 (TM 11A) have been shown to have key roles in Na^+ coupling and translocation (28).

In the absence of a crystal structure, molecular strategies employing substituted cysteine accessibility method (SCAM) analysis provides a powerful approach to systematically investigate membrane protein architecture and structure/function relationships (29). Pioneered by studies of *E. coli* LacY lactose permease (30), human transporters investigated by this methodology include the equilibrative glucose transporter GLUT1 (31, 32), the Cl^-/HCO_3^- exchanger AE1 (33–35), the Na^+/H^+ exchanger NHE1 (36), and, most recently, hCNT3 (37, 38).

To avoid confounding background reactivity with endogenous cysteine residues, SCAM analysis requires construction of a functional cysteineless version of the transporter to serve as a template for subsequent cysteine reinsertion at defined positions. In the case of hCNT3, the protein was engineered by mutation of all 14 endogenous cysteine residues to serine, resulting in the cysteineless construct hCNT3C− (37). Expressed in yeast, hCNT3C− was used to assess residues in TMs 11–13 for accessibility to methanethiosulfonate reagents (37). More recently, hCNT3C−, expressed in *Xenopus* oocytes, was used to identify a H^+-mediated conformational shift that allows access of *p*-chloromercuribenzene sulfonate (PCMBS) to specific residues in TM 12 under acidified conditions (38). One of these conformationally mobile amino acids, native cysteine residue 561, was fully protected against PCMBS inhibition by micromolar concentrations of extracellular uridine, suggesting likely proximity to the nucleoside binding pocket. In the present study, we have utilized heterologous expression in *Xenopus* oocytes, cell surface biotinylation, and site-directed mutagenesis in combination with radioisotope flux and presteady- and steady-state electrophysiological kinetic experiments to undertake an in depth functional comparison between wild-type and cysteineless hCNT3. The present investigation, which validates hCNT3C− as a template for SCAM analyses of CNTs, reveals that Cys-561 modulates Na^+- as well as H^+-coupled modes of hCNT3 nucleoside transport.

EXPERIMENTAL PROCEDURES

Site-directed Mutagenesis and DNA Sequencing—hCNT3 DNA (GenBank™ accession number AF305210) provided the template for the construction of a cysteineless version of hCNT3 (hCNT3C−) with all 14 endogenous cysteine residues converted to serine (37). hCNT3C− was transferred from the yeast *E. coli* shuttle vector pYPGE15 (37) into the *Xenopus* oocyte expression vector pGEM-HE. The latter provides additional 5′- and 3′-untranslated regions from the *Xenopus* β-globin gene, resulting in greater protein expression and functional activity when produced in *Xenopus laevis* oocytes (39). Wild-type hCNT3C and hCNT3C−, both in pGEM-HE, provided the templates for construction of corresponding mutants by the oligonucleotide-directed technique (40), using reagents from the QuikChange® site-directed mutagenesis kit (Stratagene) according to the manufacturer's directions. All constructs were sequenced in both directions by Taq DyeDeoxy terminator cycle sequencing to ensure that only the correct mutation(s) had been introduced.

Production of Recombinant Transport Proteins in Xenopus Oocytes—hCNT3 and hCNT3C− DNAs were transcribed with T7 polymerase using the mMESSAGE mMACHINE™ (Ambion) transcription system and produced in oocytes of *X. laevis* by standard procedures (41). Healthy defolliculated stage VI oocytes were microinjected with 20 nl of water or 20 nl of water containing RNA transcript (20 ng) and incubated in modified Barth's medium (changed daily) at 18 °C for 72 h prior to the assay of transport activity.

Radioisotope Flux Assays—Transport assays were performed as described previously (27, 41, 42). Groups of 12 oocytes were incubated at room temperature (20 °C) in 200 μl of transport medium containing 100 mM NaCl, 2 mM KCl, 1 mM $CaCl_2$, 1 mM $MgCl_2$, and 10 mM HEPES (pH ≥ 7.0) or 10 mM MES (pH ≤ 6.5). In experiments examining the H^+ dependence of transport, 100 mM NaCl was replaced with 100 mM ChCl. ChCl also substituted for NaCl in Na^+ activation experiments. Except where otherwise indicated, the nucleoside concentration was 10 μM. Uptake was traced with ^{14}C- or ^3H-radiolabeled nucleosides (1 or 2 μCi/ml, respectively) (GE Healthcare) using a 1-min uptake interval to measure initial rates of transport (influx). In experiments with adenosine, 1 μM deoxycoformycin was added to inhibit breakdown by adenosine deaminase. At the end of the incubation period, extracellular label was removed by six rapid washes in ice-cold Na^+-free, ChCl transport medium (pH 7.5), and individual oocytes were dissolved in 1% (w/v) SDS for quantitation of cell-associated radioactivity by liquid scintillation counting (LS 6000 IC; Beckman). The flux values shown are means ± S.E. of 10–12 oocytes, and each experiment was performed at least twice on different batches of cells. Values for mediated transport were calculated as uptake in RNA-injected oocytes *minus* uptake in control oocytes injected with water alone. Kinetic parameters (K_m, K_{50}, V_{max},

Hill coefficient) ± S.E. were calculated from data for mediated transport using SigmaPlot software (Jandel Scientific Software).

Electrophysiology—Steady-state and presteady-state hCNT3 and hCNT3C− membrane currents were measured at room temperature (20 °C) using the whole cell, two-electrode voltage clamp technique (GeneClamp 500B; Molecular Devices Corp.), as described previously (16–18). The GeneClamp 500B was interfaced to an IBM-compatible PC via a Digidata 1322A A/D converter and controlled by pCLAMP software (version 9.0; Molecular Devices Corp.). The microelectrodes were filled with 3 M KCl and had resistances ranging from 0.5 to 1.5 megaohms. Following microelectrode penetration, resting membrane potential was measured over a 10-min period prior to the start of the experiment. Oocytes exhibiting an unstable membrane potential or a potential more positive than −30 mV were discarded. Individual oocytes with good resting membrane potentials were clamped at −50 mV. Steady-state currents were measured using a uridine concentration of 100 μM. In Na^+ activation experiments, uridine-evoked currents from six or more oocytes from the same batch of oocytes used on the same day were individually normalized and averaged to produce mean values ± S.E.

Presteady-state (transient) currents were studied using a voltage pulse protocol, as described previously (16). Membrane voltage was stepped from the holding potential (V_h) of −50 mV to a range of test potentials (V_t) from −150 to +75 mV in 25-mV increments. The voltage rise time of the clamp was adjusted by use of an oscilloscope such that it varied between 200 and 500 μs. Current signals were measured in medium of the same composition used in radioisotope flux assays and filtered at 2 kHz (four-pole Bessel filter) at a sampling interval of 200 μs/point (corresponding to a sampling frequency of 5 kHz). For data presentation, representative traces were averaged from two pulses for which the current at each test potential was averaged from five sweeps and further filtered at 0.75 kHz by pCLAMP 9.0 software (Molecular Devices Corp.).

Charge/Nucleoside Stoichiometry—Na^+/nucleoside and H^+/nucleoside coupling ratios for hCNT3C− were determined by simultaneously measuring Na^+ or H^+ currents and 100 μM [^{3}H]uridine (2 μCi/ml) uptake under voltage clamp conditions, as described above. Individual hCNT3C−-producing oocytes were placed in a perfusion chamber and voltage-clamped at −90 mV in the appropriate nucleoside-free medium for a 10-min period to monitor base-line currents. When the base line was stable, the nucleoside-free medium was exchanged with medium of the same composition containing radiolabeled uridine. Current was measured for 30 s, and uridine uptake was terminated by washing the oocyte with nucleoside-free medium until the current returned to base line. The oocyte was then transferred to a scintillation vial and solubilized with 1% (w/v) SDS for quantitation of oocyte-associated radioactivity. Nucleoside-induced current was obtained as the difference between base-line current and the inward uridine current. The total charge translocated into the oocyte during the uptake period was calculated from the current-time integral and correlated with the measured radiolabeled flux for each oocyte to determine the charge/uptake ratio. Basal [^{3}H]uridine uptake was determined in control water-injected oocytes (from the same donor frog) under equivalent conditions and used to correct for endogenous nonmediated uridine uptake over the same incubation period. Coupling ratios ± S.E. were calculated from slopes of least squares fits of uridine-dependent charge *versus* uridine accumulation for eight or more oocytes.

Cell Surface Expression and Glycosylation—Production of recombinant hCNT3 and hCNT3C− proteins at the oocyte cell surface was determined by labeling of intact oocytes with EZ-Link sulfo-NHS-LC-biotin (Pierce), followed by isolation of the resultant biotinylated plasma membrane proteins using immobilized streptavidin resin (Pierce) according to the manufacturer's instructions. Glycosylation status was established by digestion with *N*-glycosidase F (Roche Applied Science). Identically treated samples omitting enzyme were used as controls.

For immunoblotting, solubilized proteins from two oocytes/lane were resolved on 12% SDS-polyacrylamide gels (43). The electrophoresed proteins were transferred to polyvinylidene difluoride membranes and probed with affinity-purified anti-hCNT3-(45–69) polyclonal antibodies (10). Blots were then incubated with horseradish peroxidase-conjugated anti-rabbit antibodies (GE Healthcare) and developed with enhanced chemiluminescence reagents (GE Healthcare).

RESULTS

As depicted in Fig. S1, hCNT3 contains 14 endogenous cysteine residues. Nine of these are located within either the extramembranous N-terminal (Cys-82, Cys-91, and Cys-94) or C-terminal (Cys-621, Cys-643, Cys-644, Cys-673, Cys-674, and Cys-684) regions of the transporter. Five are positioned in predicted TMs (Cys-121 in TM 1, Cys-486 in TM 11, Cys-561 in TM 12, and Cys-602 and Cys-607 in TM 13). To enable transmembrane protein topology mapping and structure/function analysis of hCNT3 by SCAM, all 14 cysteine residues of hCNT3 were mutated to serine. The resulting cysteineless version of hCNT3 (hCNT3C−) was capable of Na^+-dependent nucleoside transport when produced in yeast and has been used as template in an initial series of SCAM analyses of hCNT3 TMs 11–13 (37, 38). The current work extended these studies by using the dual radioisotope flux and electrophysiological capabilities of the *Xenopus* oocyte heterologous expression system to undertake a detailed functional characterization of hCNT3C−.

hCNT3C− Nucleoside Selectivity and Cation Dependence—The experiment of Fig. 1*A* investigated the ability of hCNT3C− to transport a panel of radiolabeled physiological pyrimidine and purine nucleosides. Since wild-type hCNT3 is both Na^+- and H^+-coupled (14, 17, 18) and since Na^+- and H^+-coupled hCNT3 exhibit different nucleoside selectivity profiles (17), the experiment was performed both in the presence of Na^+ and H^+ (100 mM NaCl, pH 7.5, and 100 mM ChCl, pH 5.5, respectively). As described under "Experimental Procedures," the flux values shown in this and subsequent experiments depict mediated transport activity, defined as the difference in uptake between RNA transcript-injected and control water-injected oocytes using a 1-min uptake interval to determine initial rates of transport (Fig. S2). Nucleoside uptake in water-injected oocytes was <0.1 pmol/oocyte·min^{-1} under all conditions tested (data not shown).

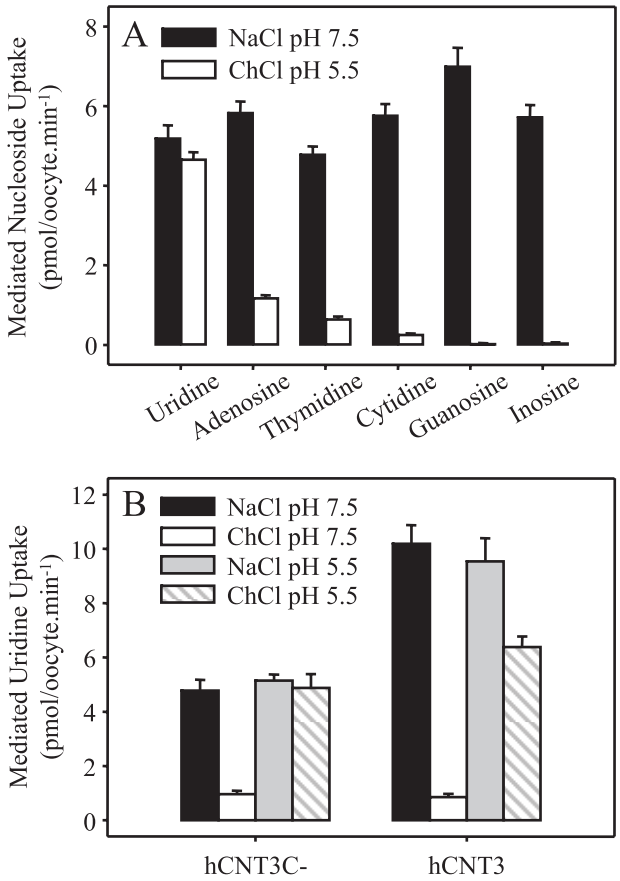

FIGURE 1. **Substrate and cation selectivity of hCNT3C−.** *A*, influx of a panel of physiological radiolabeled nucleosides (10 μM) by oocytes producing hCNT3C− was measured under initial rate conditions (1-min flux) in transport medium containing 100 mM NaCl, pH 7.5 (*black* bars), or ChCl, pH 5.5 (*white* bars). *B*, influx (1 min) of 10 μM radiolabeled uridine by wild-type hCNT3 or hCNT3C− was measured in transport medium containing 100 mM NaCl, pH 7.5 (*black* bars), ChCl, pH 7.5 (*white* bars), NaCl, pH 5.5 (*gray* bars), or ChCl, pH 5.5 (*hatched* bars). Values (*A* and *B*) were corrected for basal nonmediated uptake in control water-injected oocytes and are means ± S.E. of 10–12 oocytes.

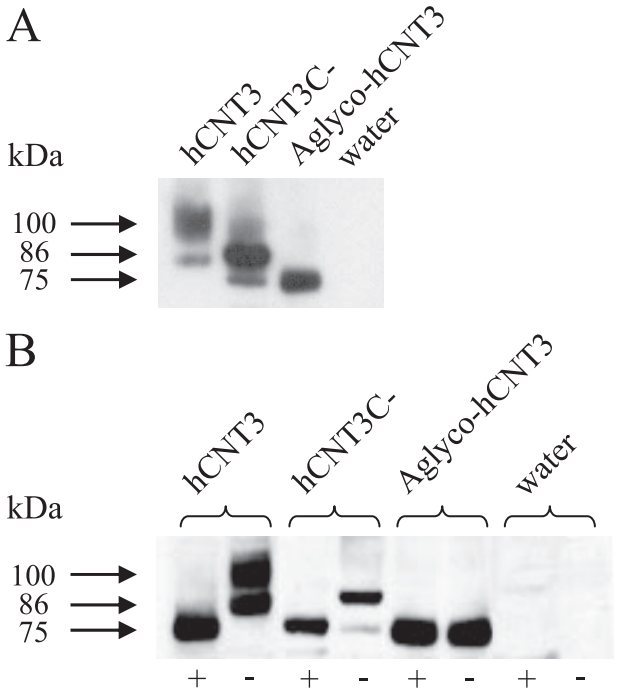

FIGURE 2. **Immunoblot analysis of hCNT3, hCNT3C−, and aglyco-hCNT3.** Labeling of oocytes with sulfo-NHS-LC-biotin was used in conjunction with immobilized streptavidin resin to separate recombinant hCNT3, hCNT3C−, and aglyco-hCNT3 cell surface immunoreactivity (*A*) from that associated with total (plasma + intracellular) membranes (*B*). Immunoblots of the fractions were probed with anti-hCNT3 antibodies. In *B*, *plus* and *minus signs* refer to digestion with *N*-glycosidase F. The positions of molecular weight standards are shown on the *left*. *Water*, control water-injected oocytes. Blots shown in *A* and *B* are from different gels.

Similar to wild-type hCNT3 (14, 23), hCNT3C− in Na^+-containing medium transported uridine, adenosine, thymidine, cytidine, guanosine, and inosine at equivalent rates (4.8–7.0 pmol/oocyte·min^{-1}). Also similar to the wild-type protein (17), this broad selectivity profile was markedly altered in H^+-containing medium (uridine ≫ adenosine, thymidine > cytidine > guanosine, inosine) with only uridine showing similar rates of transport in the two media. The different nucleoside selectivity profiles of Na^+- and H^+-coupled hCNT3 and hCNT3C− suggest that Na^+- and H^+-bound versions of the transporters have significantly different conformations of the nucleoside binding pocket and/or translocation channel (17). Only the H^+-coupled form of hCNT3 is susceptible to inhibition by the hydrophilic thiol-reactive agent PCMBS (38).

Fig. 1*B* compares the cation dependence of hCNT3 and hCNT3C− influx of 10 μM ^{14}C-labeled uridine in the presence of Na^+ and/or H^+ (100 mM NaCl or ChCl, pH 7.5 or 5.5, as indicated). Like hCNT3, hCNT3C− displayed high levels of uridine uptake in the presence of Na^+ (NaCl, pH 7.5), H^+ (ChCl, pH 5.5), and both Na^+ and H^+ (NaCl, pH 5.5). Relative to hCNT3, hCNT3C− exhibited an equivalent rate of uridine transport in the presence of H^+ (ChCl, pH 5.5) but did not show the wild-type increase in uridine influx in the presence of Na^+ (NaCl, pH 7.5) or Na^+ plus H^+ (NaCl, pH 5.5). As a result, the ratio of uridine influx in the presence of Na^+ (NaCl, pH 7.5) to that in the presence of H^+ (ChCl, pH 5.5) decreased from 1.60 for wild-type protein to 0.98 for hCNT3C−. These uridine uptake ratios are in good agreement with that reported previously for hCNT3 (17) and with the other results for hCNT3C− shown in Fig. 1*A*. The residual uridine fluxes evident in the absence of Na^+ and at a low H^+ concentration (ChCl, pH 7.5) can be attributed to the small but significant amount of H^+ activation that occurs under these conditions (17).

Cell Surface Expression and Glycosylation of hCNT3C—The equivalent levels of transport activity shown in Fig. 1*B* suggest that hCNT3 and hCNT3C− were present in oocyte plasma membranes in similar quantities. This was investigated directly by cell surface labeling with sulfo-NHS-LC-biotin using immobilized streptavidin resin to separate cell surface protein (Fig. 2*A*) from that associated with total (plasma + intracellular) membranes (Fig. 2*B*). Immunoblots of the fractions were probed with hCNT3 polyclonal antibodies (10) directed against amino acid residues 45–69 of the extramembranous N-terminal region of the protein (Fig. S1). To evaluate the glycosylation status of hCNT3 and hCNT3C−, the immunoblots in Fig. 2, *A* and *B*, also include aglyco-hCNT3, a construct produced by mutating all four potential N-terminal glycosylation acceptor sites, asparagine residues 630, 636, 664, and 678, to aspartate (Fig. S1). For comparison with the electrophoretic mobility of aglyco-hCNT3, Fig. 2*B* also shows the same streptavidin fractions of total hCNT3 and hCNT3C−

TABLE 1

Uridine kinetic parameters for hCNT3 and hCNT3C−

Radiolabeled 10 μM uridine influx was measured in 100 mM NaCl transport medium, pH 7.5, and 100 mM ChCl transport medium, pH 5.5, under initial rate conditions (1-min) in oocytes producing hCNT3 and hCNT3C−. Kinetic parameters were calculated from data shown in Fig. S3 corrected for basal (nonmediated) uptake in control water-injected oocytes.

	Apparent K_m value	V_{max}	V_{max}/K_m ratio
	μM	*pmol/oocyte·min*$^{-1}$	
hCNT3			
NaCl, pH 7.5	14.7 ± 1.7	22.7 ± 0.7	1.54 ± 0.12
ChCl, pH 5.5	62.4 ± 5.4	53.1 ± 1.1	0.85 ± 0.11
hCNT3C−			
NaCl, pH 7.5	18.4 ± 1.5	12.4 ± 0.2	0.67 ± 0.11
ChCl, pH 5.5	63.4 ± 5.1	23.2 ± 0.4	0.37 ± 0.11

membranes before and after digestion with *N*-glycosidase F. Antibody specificity was evaluated in membrane fractions prepared from control water-injected oocytes.

Consistent with the presence of multiple possible sites of *N*-linked glycosylation, cell surface hCNT3 and hCNT3C− exhibited three discreet immunobands at 100, 86, and 75 kDa (Fig. 2*A*). Total cell surface immunoreactivity was similar for the two transporters, the majority of hCNT3 and hCNT3C− staining being associated with the highest and intermediate molecular weight forms, respectively (Fig. 2*A*). Corresponding patterns of immunoreactivity were apparent in total membranes (Fig. 2*B*). Indicative of proper protein folding; therefore, hCNT3C− was processed to the oocyte plasma membrane in amounts similar to wild-type hCNT3. Digestion with *N*-glycosidase F shifted hCNT3 and hCNT3C− immunoreactivity to the lower molecular mass band at 75 kDa, an electrophoretic mobility identical to that of aglyco-hCNT3 and in good agreement with the molecular mass of hCNT3 calculated from its amino acid sequence (77 kDa). Confirming antibody specificity for hCNT3/hCNT3C−, no immunoreactivity was detected in blots from control water-injected oocytes.

Kinetic Characterization of hCNT3C—To further investigate hCNT3C− function, the concentration dependence of radiolabeled uridine (0–1 mM) influx by hCNT3 and hCNT3C− was measured either in the presence of Na^+ (100 mM NaCl, pH 7.5) or in the presence of H^+ (100 mM ChCl, pH 5.5) (Fig. S3). The corresponding kinetic parameters are given in Table 1. The results demonstrate robust high affinity transport of uridine by hCNT3C−. Similar to hCNT3 and in agreement with previous kinetic data for the wild-type transporter (17), the apparent K_m value of hCNT3C− for uridine in Na^+-containing transport medium was lower than that in the presence of H^+ (15 and 62 μM, respectively, for hCNT3 compared with 18 and 63 μM, respectively, for hCNT3C−). Calculated uridine V_{max}/K_m ratios, an indicator of transporter efficiency and a kinetic predictor of relative transport rates at permeant concentrations less than K_m values, were consistent with the 10 μM influx data shown in Fig. 1*B* (hCNT3(Na^+) > hCNT3(H^+), hCNT3C−(Na^+), and hCNT3C−(H^+)).

Cation activation curves were also determined for both transporters using a radiolabeled uridine concentration of 10 μM. Na^+ activation was measured over the concentration range 0–100 mM NaCl in transport medium at pH 7.5 and 8.5 (Fig. 3, *A* and *B*, respectively), the latter to eliminate the small amount of H^+ activation that occurs at neutral pH (17). Isosmolarity was maintained with ChCl. H^+ activation was measured in 100 mM ChCl transport medium at pH values ranging from 4.5 to 8.5 (Fig. 3*C*). Kinetic parameters derived from these data are presented in Tables 2 and 3 (Na^+ and H^+, respectively). Reflecting previously reported differences in Na^+ and H^+ cou-

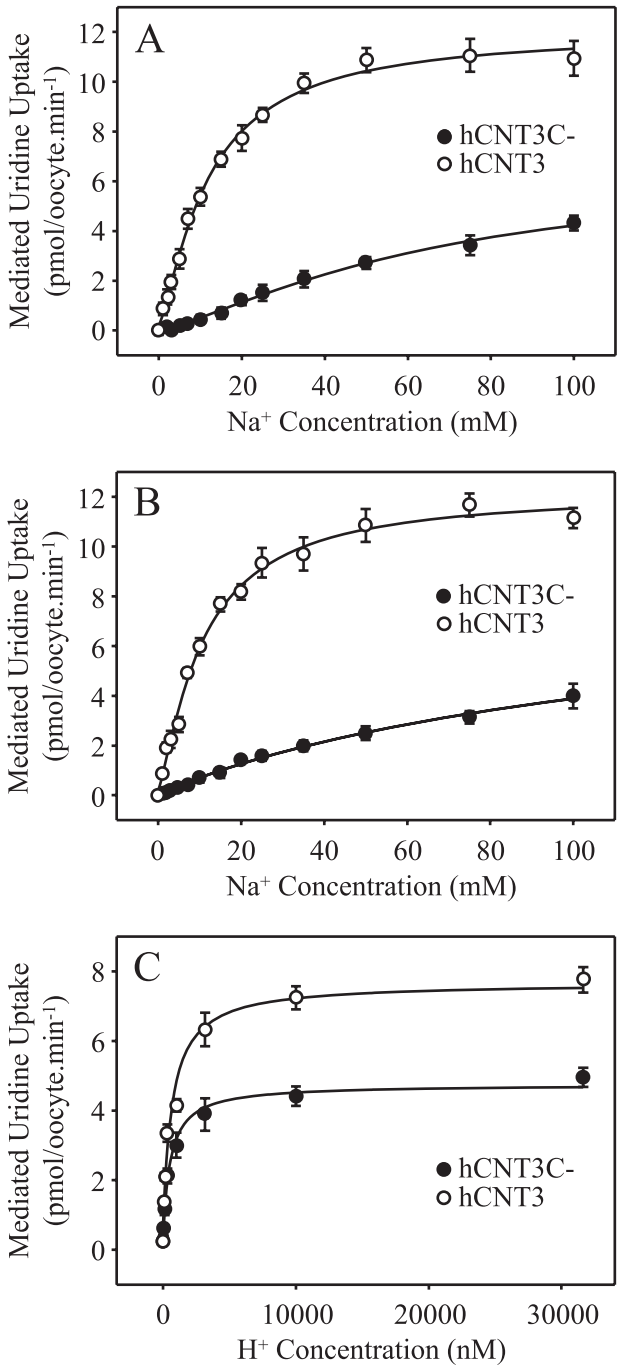

FIGURE 3. **Na^+ and H^+ activation kinetics of oocytes producing hCNT3 and hCNT3C−.** Na^+ activation curves for oocytes producing hCNT3 (*open circles*) and hCNT3C− (*filled circles*) were measured in transport medium containing 0–100 mM NaCl at pH 7.5 (*A*) and pH 8.5 (*B*), with isosmolarity maintained by the addition of ChCl. Corresponding H^+ activation curves were determined in 100 mM ChCl transport medium at pH values ranging from 4.5 to 8.5 (*C*). The radiolabeled uridine concentration was 10 μM (1-min flux). Corrected for basal (nonmediated) uptake in control water-injected oocytes, each value is the mean ± S.E. of 10–12 oocytes. Error bars are not shown where values were smaller than that represented by the *symbols*. Kinetic parameters calculated from the data are presented in Tables 2 and 3.

TABLE 2
Na^+ activation kinetic parameters for hCNT3, hCNT3C−, and mutants

	Apparent K_{50} value	V_{max}	Hill coefficient
	mM	*pmol/oocyte·min*$^{-1}$	
hCNT3,[a] pH 7.5	12.0 ± 0.8	11.9 ± 0.5	1.4 ± 0.1
hCNT3,[a] pH 8.5	10.7 ± 1.0	12.0 ± 0.7	1.4 ± 0.1
hCNT3C−,[a] pH 7.5	>40	ND[b]	
hCNT3C−,[a] pH 8.5	>40	ND	
S486C(C−),[c] pH 8.5	>40	ND	
S561C(C−),[c] pH 8.5	7.2 ± 0.6	6.0 ± 0.3	1.4 ± 0.1
S602C(C−),[c] pH 8.5	>40	ND	
S607C(C−),[c] pH 8.5	>40	ND	
C561S,[d] pH 8.5	>40	ND	
C561G,[e] pH 8.5	>40	ND	
C561A,[e] pH 8.5	10.7 ± 0.6	6.9 ± 0.2	1.5 ± 0.1
C561V,[e] pH 8.5	31.3 ± 1.9	9.1 ± 0.4	1.4 ± 0.1
C561T,[e] pH 8.5	>40	ND	
C561I,[e] pH 8.5	>40	ND	
S561A(C−), [d] pH 8.5	20.5 ± 0.9	6.0 ± 0.2	1.4 ± 0.1

[a] From Fig. 3, *A* and *B*.
[b] ND, could not be determined; in 100 mM transport medium with 0–100 mM NaCl (pH 7.5 or 8.5, as indicated, isosmolarity maintained by ChCl).
[c] From Fig. 7, *A–D*.
[d] From Fig. 8*A*.
[e] Data not shown.

TABLE 3
H^+ activation kinetic parameters for hCNT3, hCNT3C−, and mutants

	Apparent K_{50} value	V_{max}	Hill coefficient
	nM	*pmol/oocyte·min*$^{-1}$	
hCNT3[a]	690 ± 200	7.0 ± 0.4	0.8 ± 0.1
hCNT3C−[a]	550 ± 100	4.4 ± 0.2	0.8 ± 0.1
S561C(C−)[b]	830 ± 150	7.1 ± 0.3	0.8 ± 0.1
C561S[c]	870 ± 80	4.7 ± 0.1	0.7 ± 0.1
C561G[b]	900 ± 90	2.5 ± 0.1	1.0 ± 0.1
C561A[b]	490 ± 100	3.5 ± 0.2	0.8 ± 0.1

[a] From Fig. 3*C*.
[b] Data not shown.
[c] From Fig. 8*B*; in 100 mM ChCl transport medium with pH values ranging from 4.5 to 8.5.

pling by hCNT3 (17, 18), the wild-type protein exhibited saturable Na^+ and H^+ activation curves that were sigmoidal and hyperbolic in nature, respectively, with apparent K_{50} values of 12 (pH 7.5) and 11 mM (pH 8.5) for Na^+ and 690 nM for H^+. Calculated Hill coefficients were consistent with 2:1 (Na^+) and 1:1 (H^+) cation/nucleoside coupling ratios. Validating the subsequent use of pH 8.5 to study Na^+ coupling of hCNT3/hCNT3C− without interference from H^+, there was no difference in hCNT3 Na^+ activation kinetics at pH 7.5 and 8.5.

In marked contrast to wild-type hCNT3 and consistent with the relative decrease in Na^+- *versus* H^+-coupled uridine transport activity noted for the cysteineless transporter in Fig. 1*B* and Table 1, the corresponding cation activation curves for hCNT3C− revealed a marked and specific decrease in apparent affinity for Na^+ (apparent K_{50} > 40 mM). This shift in Na^+ affinity did not extend to H^+, since kinetic parameters for hCNT3C− H^+ activation were comparable with those of hCNT3 (apparent K_{50} value of 550 nM). Similarly, the corresponding Hill coefficient was consistent with a H^+/nucleoside coupling ratio of 1:1. That for Na^+ could not be determined, although the curve appeared sigmoidal (Fig. 3, *A* and *B*) and therefore potentially consistent with the wild-type Na^+/nucleoside coupling ratio of 2:1. Similar to the wild-type protein, there was no difference in hCNT3C− Na^+ activation kinetics at pH 7.5 and 8.5. All subsequent hCNT3/hCNT3C− Na^+ activation and Na^+ coupling experiments were performed at pH 8.5.

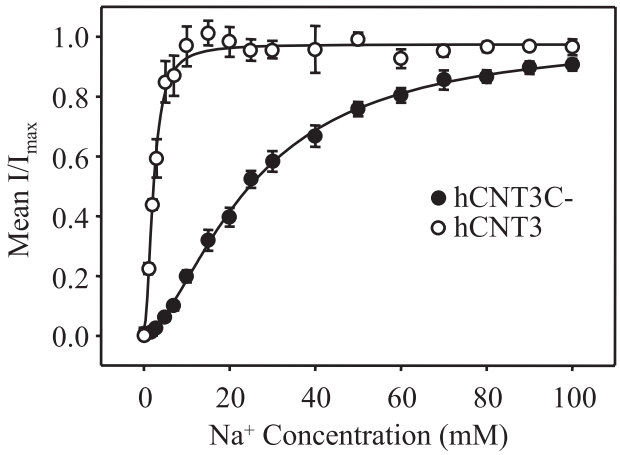

FIGURE 4. **Na^+ activation kinetics of hCNT3 and hCNT3C− determined by electrophysiology.** Na^+ activation curves for hCNT3 (*open* circles) and hCNT3C− (*solid* circles) were determined at a holding potential of −90 mV in transport medium of the same composition used in radioisotope flux studies (Fig. 3*B*). The uridine concentration was 100 μM. Uridine-evoked currents at each Na^+ concentration were normalized to the respective fitted I_{max} value and are presented as the mean ± S.E. of 6–8 oocytes. Error bars are not shown where values were smaller than that represented by the *symbols*. No currents were detected in control water-injected oocytes (data not shown).

Electrophysiological Determination of hCNT3C− Na^+ Activation Kinetics—Since hCNT3 is electrogenic, the Na^+ activation kinetic parameters of hCNT3C− were also determined by electrophysiology. Fig. 4 depicts the relationship between Na^+ concentration and 100 μM uridine-evoked current for oocytes expressing wild-type hCNT3 or hCNT3C− clamped at a membrane holding potential of −90 mV. Oocytes were individually normalized to their predicted I_{max} values and subsequently averaged to produce mean kinetic parameters. In agreement with previous studies (17, 18), the apparent K_{50} value for Na^+-coupled uridine uptake by hCNT3 under these conditions was 2.2 ± 0.1 mM. Similar to the radioisotope flux data in Fig. 3, *A* and *B*, hCNT3C− exhibited a marked decrease (~11-fold) in the apparent affinity for Na^+ in comparison with that of the wild-type protein, with an increased apparent K_{50} value of 24.7 ± 0.8 mM. The corresponding Hill coefficients for hCNT3C− and hCNT3 were ≥1.5, suggesting that the wild-type Na^+/uridine stoichiometry of 2:1 was maintained by hCNT3C−. The apparent K_{50} values for hCNT3 and hCNT3C− as determined by electrophysiology were lower than those derived from radioisotope flux data because of (i) the different uridine concentrations used in the two studies (100 and 10 μM, respectively) and (ii) the difference in membrane potential in the two situations (−90 mV for the voltage-clamped oocytes *versus* ~−40 mV under radioisotope flux conditions) (17).

Presteady-state Electrophysiology of hCNT3C—Presteady-state electrophysiological experiments were performed on oocytes producing hCNT3C− voltage-clamped at a holding potential (V_h) of −50 mV. Presteady-state currents were activated by voltage steps to a series of test potentials (V_t) in the presence of varying concentrations of Na^+ (0–100 mM NaCl, pH 8.5; Fig. 5, *A–E*) and in the presence of both Na^+ and extra-

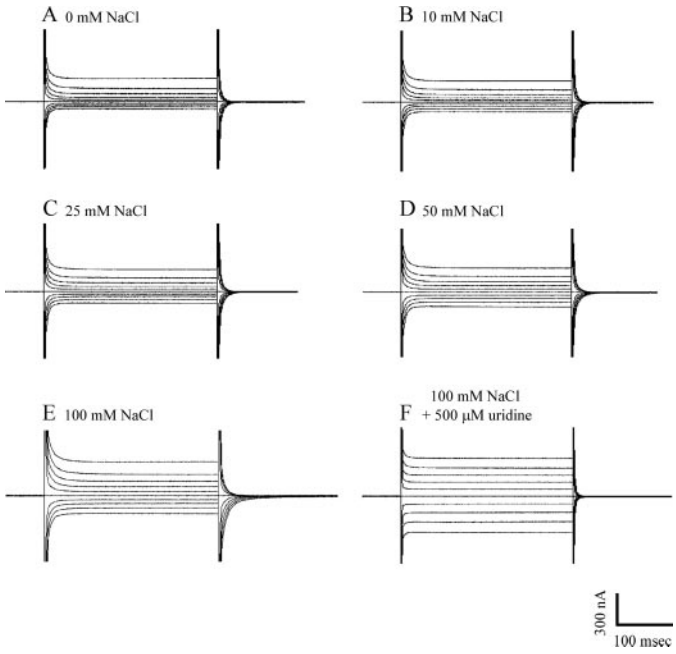

FIGURE 5. **Presteady-state currents of hCNT3C−.** Oocytes expressing hCNT3C− were held at a holding potential (V_h) of −50 mV and stepped to a range of test potentials (V_t) from −150 to +75 mV in 25-mV increments. Representative traces from a single oocyte are shown in transport medium containing 0 mM NaCl, pH 8.5 (100 mM ChCl, pH 8.5; *A*); 10, 25, 50, and 100 mM NaCl, pH 8.5 (*B–E*, respectively); and 100 mM NaCl, pH 8.5, plus 500 μM uridine (*F*).

cellular uridine (100 mM NaCl, pH 8.5, plus 500 μM uridine; Fig. 5*F*). hCNT3C− exhibited presteady-state currents similar to those previously described for wild-type hCNT3 (17) and wild-type hCNT1 (16), which increased in magnitude upon exposure to extracellular Na^+ and were largely eliminated upon the addition of uridine. However, consistent with a reduced binding affinity for Na^+ and different from the wild-type protein, presteady-state currents approached maximum values only at Na^+ concentrations of >50 mM, a behavior also observed for hfCNT, another CNT with low apparent affinity for Na^+.[5] Presteady-state currents were absent from control water-injected oocytes (data not shown) (16, 28).

Na^+/Uridine and H^+/Uridine Stoichiometry—The Na^+/uridine and H^+/uridine stoichiometries of hCNT3C− were determined directly by simultaneous measurement of uridine-evoked currents and 100 μM radiolabeled uridine uptake under voltage clamp conditions, as described previously (16, 17). A representative current trace is depicted in Fig. 6*A* for an oocyte expressing hCNT3C− exposed to 100 μM radiolabeled uridine in 100 mM NaCl transport medium, pH 8.5. Presented in Fig. 6, *B* and *C*, each data point represents a single oocyte, and the coupling ratio is given by the slope of the linear fit of charge (pmol) *versus* uptake (pmol). In 100 mM NaCl transport medium (pH 8.5) and at a holding potential of −90 mV, the linear correlation between uridine-dependent charge and uridine accumulation gave an Na^+/uridine coupling ratio of 2.08 ± 0.11 (Fig. 6*B*). The corresponding H^+/uridine stoichiometry was determined in acidified 100 mM ChCl transport medium (pH 5.5) and resulted in a coupling ratio of 1.11 ± 0.06 (Fig. 6*C*). Both hCNT3C− stoichiometries agree with previously published values for hCNT3 (17, 18) and with the Hill coefficients derived from hCNT3 and hCNT3C− from Figs. 3 and 4 (Tables 2 and 3).

Cation Activation of Aglyco-hCNT3—The experiment of Fig. 2 demonstrated that wild-type hCNT3 and hCNT3C− have different patterns of *N*-linked glycosylation. To exclude the possibility that the shift in hCNT3C− Na^+ affinity was secondary to the altered glycosylation status of the protein, the apparent K_{50} and V_{max} values for Na^+ and H^+ activation of aglyco-hCNT3 were determined under conditions identical to those used in Fig. 3*B* for hCNT3C−. Kinetic parameters for both cations were not significantly different from those of the wild-type protein measured in parallel in the same experiment (aglyco-hCNT3 and hCNT3 apparent K_{50} and V_{max} values of 10.5 ± 1.1 and 8.8 ± 1.2 mM and 6.8 ± 0.4 and 7.4 ± 0.5 pmol/oocyte·min^{-1}, respectively, for Na^+ and 399 ± 98 and 506 ± 182 nM and 4.7 ± 0.2 and 5.3 ± 0.4 pmol/oocyte·min^{-1}, respectively, for H^+) (cation activation curves not shown).

Cation Activation of hCNT3C− Mutants—The hCNT3C− construct differs from wild-type hCNT3 by the replacement of all 14 endogenous cysteine residues with serine. Five of these substitutions lie within predicted TM regions of the protein (supplemental Fig. S1). Of these, four reside in the C-terminal half of the protein, which corresponds to the region that chimeric studies between hCNT1 and hCNT3 (17) and between hCNT1 and hfCNT (19) have demonstrated to be responsible for Na^+ coupling. Site-directed mutagenesis experiments to identify the residue(s) responsible for the shift in hCNT3C− Na^+ affinity therefore focused on the four C-terminal intramembranous cysteine residues: Cys-486 (TM 11), Cys-561 (TM 12), Cys-602 (TM 13), and Cys-607 (TM 13). In the hCNT3C− background, cysteine residues were individually reintroduced at each of these positions, yielding constructs S486C(C−), S561C(C−), S602C(C−), and S607C(C−). Measured under conditions identical to those used in Fig. 3*B*, Fig. 7 shows oocyte Na^+ activation curves for each mutant. Corresponding kinetic parameters are given in Table 2. S486C(C−), S602C(C−), and S607C(C−) (Fig. 7, *A*, *C*, and *D*) each retained Na^+ activation curves similar to that of hCNT3C− (Fig. 3*B*), with apparent K_{50} values of >40 mM. In contrast, the Na^+ activation curve for S561C(C−) (Fig. 7*B*) closely resembled that of wild-type hCNT3 (Fig. 3*B*) with an apparent K_{50} value of 7.2 ± 0.6 mM. H^+ activation kinetics were also determined for S561C(C−), yielding apparent K_{50} and V_{max} values that were similar to those of both hCNT3C− and hCNT3 (cation activation curve not shown; Table 3).

Cation Activation of hCNT3 Mutant C561S—To confirm the role of Cys-561 in the shift in Na^+ affinity of hCNT3C−, serine was substituted for cysteine in wild-type hCNT3, creating the mutant protein C561S. Na^+ and H^+ activation kinetics for oocytes producing C561S were determined under experimental conditions identical to those described above for other hCNT3/hCNT3C− constructs and are depicted in Fig. 8. Kinetic parameters derived from the curves are presented in Tables 2 and 3. Similar to hCNT3C− (Fig. 3, *B* and *C*), C561S exhibited

[5] M. D. Slugoski, K. M. Smith, R. Mulinta, A. M. L. Ng, S. Y. M. Yao, E. L. Morrison, Q. O. T. Lee, J. Zhang, E. Karpinski, C. E. Cass, S. A. Baldwin, and J. D. Young, unpublished observation.

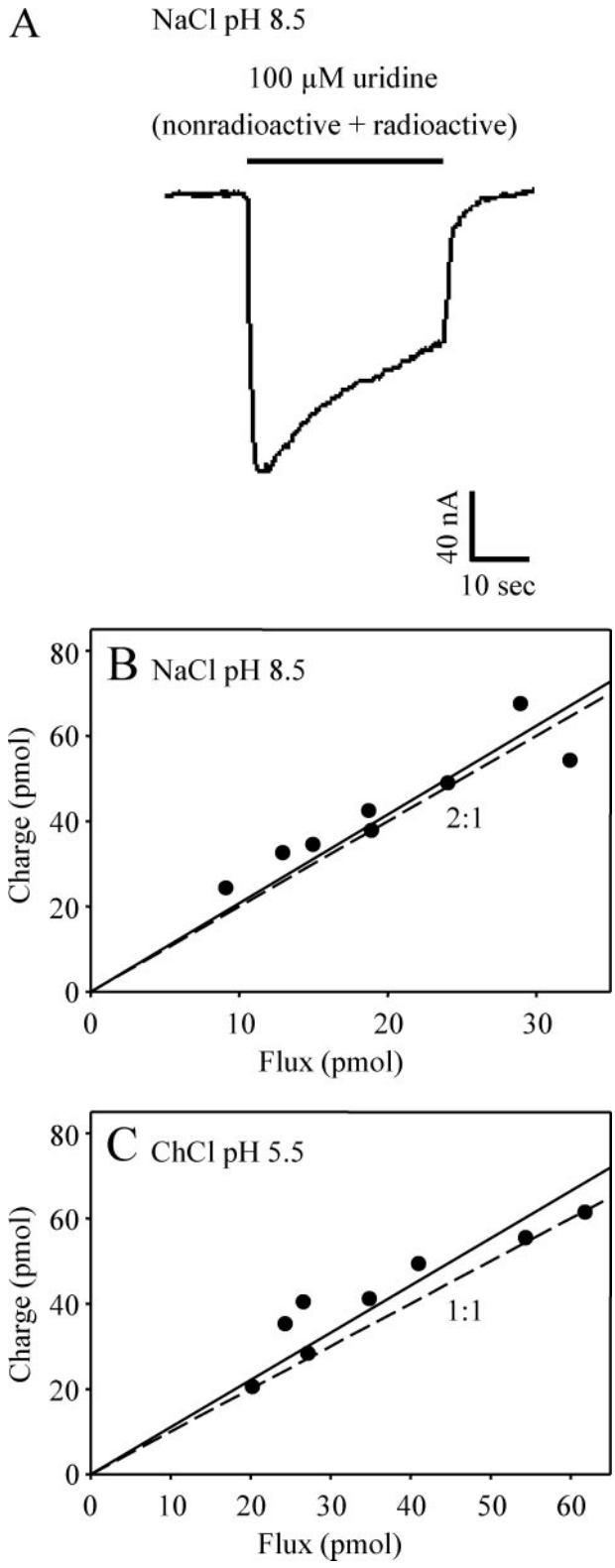

FIGURE 6. **Na^+/uridine and H^+/uridine stoichiometry of hCNT3C−.** *A*, a representative current trace for an oocyte expressing hCNT3C− clamped at a membrane potential of −90 mV and exposed to 100 μM radiolabeled uridine in 100 mM NaCl, pH 8.5. Integration of the uridine-evoked current over the uptake period yielded the charge moved; this charge, representing net cation influx, was correlated to the net uptake (*Flux*) of radiolabeled uridine by the oocyte during the same time interval. Following the same protocol (V_h of −90 mV; 100 μM uridine), *B* and *C* show charge/flux ratio plots generated for oocytes producing hCNT3C− in either 100 mM NaCl transport medium at pH 8.5 (*B*) or ChCl transport medium at pH 5.5 (*C*). Each point represents a single oocyte. Linear regression fits of both data sets passed through the origin and are indicated by *solid lines*. The *dashed lines* represent theoretical 2:1 (*B*) and 1:1 (*C*) charge/uptake ratios.

a decreased apparent affinity for Na^+ (>40 mM) in the absence of a parallel shift in H^+ apparent binding affinity.

Cation Activation of hCNT1 and hCNT1 Mutant C540S—In contrast to hCNT3, which is both H^+- and Na^+-coupled and exhibits H^+/nucleoside and Na^+/nucleoside stoichiometries of 1:1 and 2:1, respectively, hCNT1 and hCNT2 are Na^+-specific and have an Na^+/nucleoside stoichiometry of 1:1 (12, 16–18). All three proteins share similar high affinities for Na^+ binding with apparent K_{50} values of ~10 mM (12, 16–18). The residue corresponding to hCNT3 Cys-561 in hCNT1 is Cys-540. To investigate the effects of a cysteine to serine mutation at this position in another CNT family member, the same change was made in hCNT1 to create the mutant protein C540S. Mutant C540S and wild-type hCNT1 were then produced in oocytes, and their Na^+ activation kinetics were investigated under experimental conditions identical to those described above for hCNT3/hCNT3C− and mutants (Fig. 9). In agreement with previous studies (12, 27), hCNT1 displayed a hyperbolic Na^+ activation curve with an apparent affinity for Na^+ of 6.6 ± 1.0 mM and a V_{max} of 4.5 ± 0.2 pmol/oocyte·min^{-1} (Fig. 9*B*). Similarly, Na^+ activation of C540S was also hyperbolic with apparent K_m and V_{max} values of 8.4 ± 1.1 mM and 4.3 ± 0.1 pmol/oocyte·min^{-1}, respectively (Fig. 9*A*). Corresponding Hill coefficients were both 1.0 ± 0.1.

Other Amino Acid Substitutions of hCNT3 Residue Cys-561—Sequence comparisons of 126 eukaryotic and prokaryotic CNT family members revealed that the residue corresponding to hCNT3 Cys-561 is highly conserved. However, in addition to cysteine (90 family members), the amino acids alanine, valine, threonine, and isoleucine were also represented at this position (four, 21, six, and five family members, respectively). Therefore, to further elucidate the role of Cys-561 in hCNT3 cation coupling, hCNT3 mutants C561A, C561V, C561T, and C561I were constructed and produced in oocytes. Substitution of hCNT3 Cys-561 with glycine, the amino acid with the smallest side chain, was also included in the series (mutant C561G). Functional activity and cation selectivity were compared with wild-type hCNT3 and mutant C561S by measuring 10 μM radiolabeled uridine influx in both Na^+- and H^+-containing transport medium (100 mM NaCl, pH 7.5 and 100 mM ChCl, pH 5.5, respectively) (Fig. 10). Similar to these transporters, C561G and C561A exhibited both Na^+- and H^+-coupled influx of radiolabeled uridine. However, relative to transport in the presence of Na^+ and in contrast to C561A, C561G exhibited reduced influx of uridine in H^+-containing medium. Extending this trend, substitution of Cys-561 with larger neutral amino acids (mutants C561V, C561T, and C561I) led to almost total abolition of uridine influx in H^+-containing medium, a finding that was confirmed for C561I by corresponding measurements of 100 μM uridine-induced steady-state currents (Fig. 11).

Kinetic parameters for Na^+ activation of C561G, C561A, C561S, C561T, C561V, and C561I, measured as described in Fig. 3*B*, are given in Table 2. Replacement of Cys-561 with residues of a similar size (C561A and C561V) allowed full (C561A)

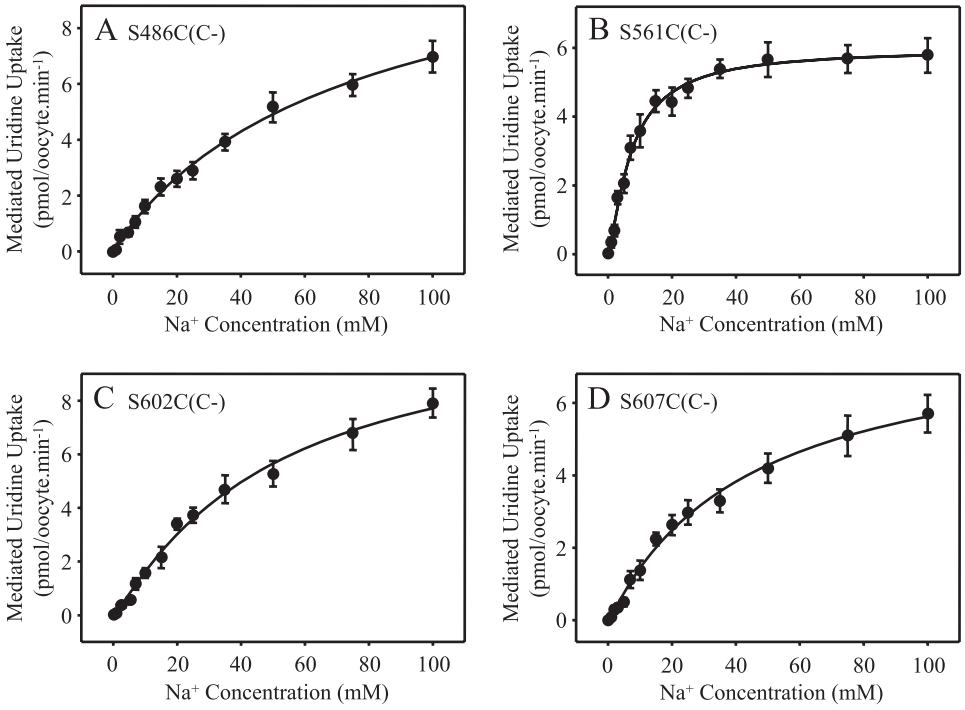

FIGURE 7. **Na^+ activation kinetics of oocytes producing hCNT3C− mutants S486C(C−) (*A*), S561C(C−) (*B*), S602C(C−) (*C*), and S607C(C−) (*D*).** Na^+ activation curves were determined as described in the legend to Fig. 3*B*. The radiolabeled uridine concentration was 10 μM (1-min flux). Corrected for basal (nonmediated) uptake in control water-injected oocytes, each value is the mean ± S.E. of 10–12 oocytes. Error bars are not shown where values were smaller than that represented by the *symbols*. Kinetic parameters calculated from the data are presented in Table 2.

or partial (C561V) recovery of Na^+ apparent affinity (K_{50} values of 10.7 ± 0.7 and 31.3 ± 1.9 mM, respectively). In contrast, C561G, C561T, and C561I exhibited reduced affinities for Na^+ similar to that of hCNT3C− (apparent K_{50} values of >40 mM). The ability of alanine to mimic cysteine at residue position 561 extended to the reciprocal hCNT3C− mutant S561A(C−), which exhibited a partially restored apparent K_{50} value of 20.5 ± 0.9 mM (Na^+ activation curve not shown; Table 2).

Corresponding kinetic parameters for H^+ activation of mutants C561G and C561A were also determined. Measured as described in Fig. 3*C* and similar to wild-type hCNT3, C561G and C561A displayed apparent K_{50} values for H^+ of 900 ± 90 and 490 ± 100 nM, respectively (H^+ activation curves not shown; Table 3).

Complementary to these cation activation analyses, we additionally determined the uridine kinetic parameters of hCNT3 mutants. Values were determined as described in Table 1 and are presented in Table 4 (concentration dependence curves not shown). In Na^+-containing transport medium (100 mM NaCl, pH 8.5), C561A and C561S exhibited high affinity for uridine similar to wild-type hCNT3 (Fig. S3 and Table 1), with apparent K_m values of 29.5 ± 2.4 and 26.5 ± 2.5 μM, respectively. In contrast, the other mutants in the series exhibited progressively increasing apparent K_m values for uridine influx: C561G (93.8 ± 16.0 μM), C561T (106 ± 27 μM), C561V (120 ± 11 μM), and C561I (216 ± 17 μM). Similar to wild-type hCNT3 (Table 1 and Fig. S3), uridine apparent K_m values increased when determined in H^+-containing transport medium (100 mM ChCl, pH 5.5). C561A (65.0 ± 6.3 μM) and C561S (91.0 ± 11.0 μM) were again comparable with the wild-type transporter, whereas C561G was higher (234 ± 32 μM).

Presteady-state Electrophysiology of hCNT3 Cys-561 and hCNT3C− S561(C−) Mutants—In a final series of experiments, presteady-state electrophysiological experiments were performed on oocytes producing the hCNT3 mutants C561A and C561S and the hCNT3C− mutant S561C(C−). As undertaken for hCNT3C− in Fig. 5, oocytes were voltage-clamped at a holding potential (V_h) of −50 mV and stepped to a series of test potentials (V_t) in the presence of varying concentrations of Na^+ (0–100 mM NaCl, pH 8.5). C561A, C561S, and S561C(C−) exhibited presteady-state currents, which increased in magnitude upon exposure to extracellular Na^+ and were eliminated following the addition of uridine (500 μM) (data not shown). Consistent with the flux demonstration that both C561A and S561C(C−) displayed high affinity for Na^+ (Table 2 and Fig. 7*B*), the profiles of the presteady-state currents as a function of Na^+ concentration resembled that of wild-type hCNT3 (17) and approached maximum values at low Na^+ concentrations consistent with their respective apparent K_{50} values for Na^+ activation (Table 2). In agreement with the decreased apparent affinity of C561S for Na^+ (Table 2 and Fig. *8A*), however, C561S presteady-state currents were similar in profile to hCNT3(C−) (Fig. 5) and hfCNT,[5] and maximal only at Na^+ concentrations of >50 mM.

DISCUSSION

hCNT3, the most recently discovered and functionally versatile of three human members of the SLC28 (CNT) protein family, is 691 amino acids in length, has a 13-TM membrane (or possibly 15-TM membrane) architecture, and utilizes electrochemical gradients of both Na^+ and H^+ to accumulate a broad range of pyrimidine and purine nucleosides and nucleoside drugs within cells (14, 15, 17, 18). Although paralogs hCNT1 and hCNT2 have a similar predicted membrane topology, they function predominantly as Na^+-coupled transporters and are pyrimidine nucleoside-preferring and purine nucleoside-preferring, respectively (12, 13, 16, 18). More widely distributed in cells and tissues than hCNT1 or hCNT2 (14) and with a central role in renal transepithelial nucleoside and nucleoside drug transport (9–11), the multifunctional capability of hCNT3 makes it the protein of choice for systematic in depth molecular characterization by SCAM. A prerequisite of this approach is the availability of a functional cysteineless version of the transporter.

Cysteineless hCNT3C−, in which all 14 endogenous cysteine residues of hCNT3 have been converted to serine, is shown

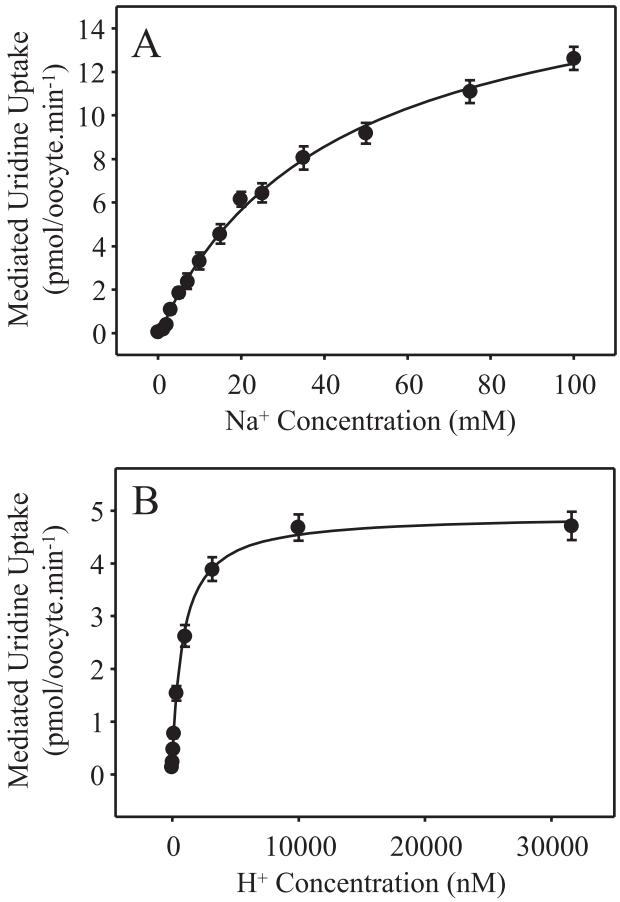

FIGURE 8. **Na^+ and H^+ activation kinetics of oocytes producing hCNT3 mutant C561S.** Na^+ (*A*) and H^+ (*B*) activation curves were determined as described in the legends to Figs. 3, *B* and *C*, respectively. The radiolabeled uridine concentration was 10 μM (1-min flux). Corrected for basal (nonmediated) uptake in control water-injected oocytes, each value is the mean ± S.E. of 10–12 oocytes. Error bars are not shown where values were smaller than that represented by the symbols. Kinetic parameters calculated from the data are presented in Tables 2 and 3.

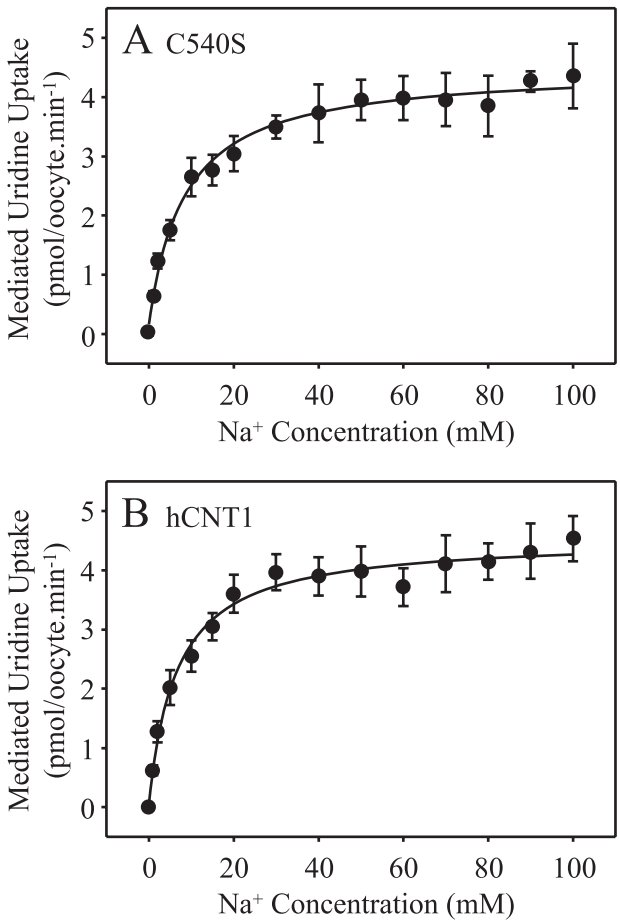

FIGURE 9. **Na^+ activation kinetics of oocytes producing hCNT1 and hCNT1 mutant C540S.** Na^+ activation curves were determined for oocytes expressing hCNT1 mutant C540S (*A*) and wild-type hCNT1 (*B*) as described in the legend to Fig. 3*B*. The radiolabeled uridine concentration was 10 μM (1-min flux). Corrected for basal (nonmediated) uptake in control water-injected oocytes, each value is the mean ± S.E. of 10–12 oocytes. Error bars are not shown where values were smaller than that represented by the *symbols*.

here to have a robust functional phenotype when produced in *Xenopus* oocytes. Similar to wild-type hCNT3 and consistent with correct folding of the cysteineless transporter, hCNT3C− exhibited broad selectivity for both pyrimidine and purine nucleosides in Na^+-containing medium (Fig. 1*A*), displayed the characteristic narrowing of this permeant selectivity in H^+-containing medium (Fig. 1*A*), was processed to the cell surface in amounts equivalent to hCNT3 (Fig. 2), exhibited apparent binding affinities for uridine in both Na^+- and H^+-containing medium similar to those of the wild-type transporter (Table 1 and Fig. S3), and retained the wild-type Na^+/uridine and H^+/uridine coupling stoichiometries of 2:1 and 1:1, respectively (Fig. 6). Recombinant hCNT3C− is also functional in yeast and was used in initial SCAM analyses to screen residues in TMs 11–13 for reactivity to methanethiosulfonate reagents (37). In oocytes, hCNT3C− was previously used in SCAM analysis of TM 12 to test residues for inhibition by PCMBS (38). Consistent with correct folding of the nucleoside binding pocket of hCNT3C−, methanethiosulfonate and PCMBS accessibility to some residues was blocked by exofacial uridine (37, 38). Taken together, these analyses validate use of

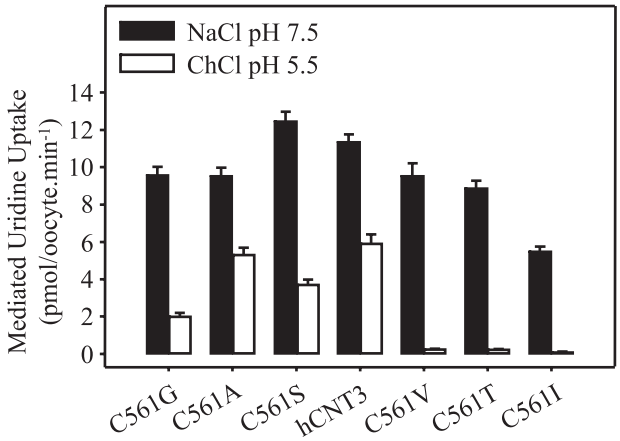

FIGURE 10. **Cation selectivity of hCNT3 mutants.** Influx of 10 μM radiolabeled uridine by hCNT3 mutants C561G, C561A, C561S, hCNT3, C561V, C561T, and C561I was measured under initial rate conditions (1 min flux) in both Na^+-containing (100 mM NaCl, pH 7.5) and H^+-containing (100 mM ChCl, pH 5.5) transport medium (*black* and *white bars*, respectively). Values were corrected for basal nonmediated uptake in control water-injected oocytes and are means ± S.E. of 10–12 oocytes. Error bars are not shown where values were smaller than that represented by the *symbols*.

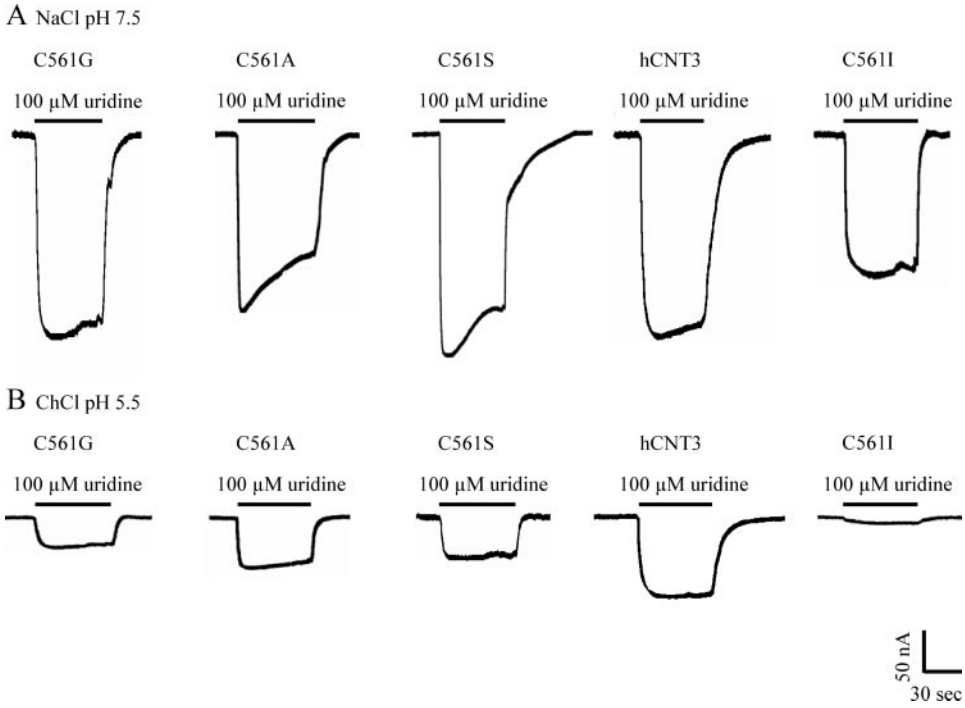

FIGURE 11. **Steady-state currents of hCNT3 mutants.** Steady-state currents were recorded for wild-type hCNT3 and mutants C561G, C561A, C561S, and C561I in oocytes that were voltage-clamped at −90 mV and exposed to 100 μM uridine in transport medium containing 100 mM NaCl, pH 7.5 (*A*), or 100 mM ChCl, pH 5.5 (*B*). No uridine-induced currents were evident in control water-injected oocytes (data not shown).

TABLE 4

Uridine kinetic parameters for hCNT3 mutants

Radiolabeled 10 μM uridine influx was measured in 100 mM NaCl transport medium, pH 8.5, and 100 mM ChCl transport medium, pH 5.5, under initial rate conditions (1 min) in oocytes producing C561G, C561A, C561S, C561V, C561T, and C561I. Kinetic parameters were calculated from data (not shown) corrected for basal (nonmediated) uptake in control water-injected oocytes.

	NaCl, pH 8.5		ChCl, pH 5.5	
	Apparent K_m value	V_{max}	Apparent K_m value	V_{max}
	μM	pmol/oocyte·min^{-1}	μM	pmol/oocyte·min^{-1}
C561G	93.8 ± 16.0	21.2 ± 1.0	234 ± 32	8.4 ± 0.4
C561A	29.5 ± 2.4	27.5 ± 0.5	65.0 ± 6.3	14.3 ± 0.4
C561S	26.5 ± 2.5	22.7 ± 0.5	91.0 ± 11.0	14.0 ± 0.5
C561V	120 ± 11	70.5 ± 2.0		
C561T	106 ± 27	74.0 ± 5.5		
C561I	216 ± 17	62.5 ± 1.7		

hCNT3C− as a template for SCAM analyses of CNT structure and function.

Characterization of hCNT3C− revealed an altered apparent affinity for Na^+; hCNT3C− and wild-type hCNT3 exhibited apparent K_{50} values for Na^+ activation of 10 μM radiolabeled uridine influx of >40 mM and 11–12 mM, respectively (Fig. 3, *A* and *B*). Under voltage clamp conditions of −90 mV with a uridine concentration of 100 μM, Na^+ activation curves for hCNT3 and hCNT3C− were sufficiently shifted to the left to establish that the change in binding affinity for Na^+ between hCNT3 and hCNT3C− was ~11-fold (apparent K_{50} values of 2.2 and 25 mM, respectively) (Fig. 4). This difference, which was also apparent in presteady-state current measurements (Fig. 5), was specific to Na^+ and did not extend to H^+ (Fig. 3*C*). The change was also specific to one particular cysteine residue, Cys-561, in TM 12. Reintroduction of cysteine at position 561 (hCNT3C− mutant S561C(C−)) restored wild-type Na^+ binding (Fig. 7), whereas the reciprocal single cysteine-to-serine substitution in hCNT3 (mutant C561S) produced an altered Na^+ binding affinity corresponding to that found for hCNT3C− (Fig. 8). Presteady-state current measurements confirmed the Na^+-binding characteristics of S561C(C−) and C561S.

Recently, a naturally occurring hCNT3 variant has been described in the Spanish population in which a T/C transition leads to the substitution of cysteine at position 602 by arginine (44). This single amino acid replacement in TM 13 led to a shift in Hill coefficient consistent with a change in Na^+/nucleoside stoichiometry from 2:1 to 1:1. In agreement with our findings here, the C602R phenotype was a consequence of the insertion of arginine at this position rather than the loss of cysteine.

Fully processed to the cell surface, hCNT3C− exhibited an altered pattern of *N*-linked glycosylation relative to that of the wild-type protein. As shown in Fig. 2, two glycosylated forms of hCNT3/hCNT3C− were apparent on SDS-polyacrylamide gels (100 and 86 kDa). Most hCNT3C− immunoreactivity was associated with the 86 kDa band, in contrast to hCNT3, for which most immunoreactivity was found in the higher molecular mass band of 100 kDa. Since no fewer than six of the 14 endogenous cysteine residues of hCNT3 are located alongside the four potential N-terminal glycosylation acceptor sites in the extracellular N-terminal tail of the protein (supplemental Fig. S1) and since these cysteines probably form intramolecular disulfide bridges within the protein, it is likely that the modified glycosylation status of the cysteineless transporter is secondary to changes in the secondary/tertiary structure of this extramembranous region of the protein. The demonstration that aglyco-hCNT3 exhibited normal Na^+ activation kinetics verified that altered glycosylation was not responsible for the shift in hCNT3C− Na^+ affinity.

As well as replacement of hCNT3 Cys-561 with serine, each of the alternative amino acids found at position 561 in other CNT family members (alanine, valine, threonine, and isoleucine) were introduced into hCNT3. To provide a more complete spectrum of neutral amino acid side chain structures in the analysis, cysteine was also mutated to glycine. In addition to cysteine, only alanine at this position (hCNT3 mutant C561A) elicited wild-type cation binding (Tables 2 and 3 and Fig. 10). The rank order of Na^+ binding affinities (cysteine and alanine > valine > glycine, serine, threonine, and isoleucine) demonstrated that normal hCNT3 Na^+ activation was critically dependent upon a combination of residue 561 side chain bulk and polarity. Tolerance of alanine at position 561 was con-

firmed in the hCNT3C− background, in that mutant S561A(C−) exhibited partially recovered Na^+ binding affinity (Table 2). Additionally, only C561A displayed wild-type hCNT3-like apparent affinities for uridine in both Na^+- and H^+-containing transport medium (Table 4). Therefore, mutation of Cys-561 to alanine instead of serine provides an alternative to hCNT3C− as template for future SCAM analyses of hCNT3 structure and function.

Despite retaining Na^+-coupled transport capability, albeit with reduced Na^+ binding affinity, substitution of Cys-561 by valine, threonine, and isoleucine had the additional and unanticipated consequence of dramatically decreasing H^+-coupled uridine transport activity (Figs. 10 and 11). Relative to Na^+, substitution of cysteine with the smaller amino acid glycine also led to reduced H^+-dependent uridine transport activity. Therefore, the nature of the amino acid side chain at position Cys-561 in hCNT3 influences both Na^+- and H^+-coupled nucleoside transport but with seemingly dissimilar structure-function profiles. For example, whereas the apparent affinity of mutant C561V for Na^+ was only moderately decreased (apparent K_{50} of 31 mM compared with 11 mM for wild-type hCNT3; Table 2), H^+-coupled uridine transport was essentially eliminated (Figs. 10 and 11). In the opposite direction, the apparent affinity of mutant C561G for Na^+ was not measurable (Table 2), whereas H^+ activation curves revealed wild-type hCNT3-like high affinity binding of H^+ (apparent K_{50} of 900 nM; Table 3). The structural requirements for Na^+ and H^+ binding and/or translocation at this single residue position are not, therefore, the same. At the level of the whole protein, other indications that Na^+ and H^+ binding and/or translocation have different structural requirements include the demonstration that hCNT3 exhibits different Na^+ and H^+ binding stoichiometries (17, 18). Na^+- and H^+-coupled hCNT3 also have markedly different nucleoside and nucleoside drug selectivities, a finding that provides evidence for two distinct cation-dependent conformational states of the protein (17). Independent of changes in cation interactions and consistent with cation/nucleoside cotransport through a common translocation pore, amino acid substitutions at position Cys-561 were also found to have a marked influence on uridine transport kinetics, increasing the uridine apparent K_m value up to 15-fold in Na^+-containing transport medium and up to 4-fold in H^+-containing transport medium (Tables 1 and 4).

In a separate study, we have independently identified Cys-561 as the cysteine residue responsible for inhibition of wild-type hCNT3 by PCMBS (38). Access of this membrane-impermeant probe to Cys-561 required H^+ but not Na^+ and was blocked by micromolar concentrations of extracellular uridine. Although this cysteine residue is conserved in Na^+-specific hCNT1 and hCNT2, neither transporter is affected by PCMBS. When converted to cysteine, two other residues in hCNT3 adjacent to Cys-561 (Ile-554 and Tyr-558) also led to H^+-activated inhibition by PCMBS (38). These findings suggest that Cys-561 is located in the translocation pore in a mobile region within or closely adjacent to the nucleoside binding pocket and that accessibility of PCMBS to this residue reports a specific H^+-induced conformational state of the protein (38). Positioned in the middle of TM 12 (Fig. S1), this residue position is now also revealed to be capable of modifying the functionality of the protein, with marked influences on both Na^+/nucleoside and H^+/nucleoside cotransport. Within the plane of the membrane, Cys-561 is located at the interface between those residues sensitive to inhibition by PCMBS in H^+-containing medium only and those where inhibition occurs in the presence of both Na^+ and H^+ (38). Remarkably intolerant to substitution by other amino acids, only cysteine replacement by alanine approached full wild-type kinetic functionality. Matching the previous observation that H^+-induced inhibition by PCMBS is specific to hCNT3 and not found in hCNT1/2 (38), we have similarly found that mutation of hCNT1 Cys-540 to serine (the cysteine substitution corresponding to hCNT3 C561S) had no influence on Na^+ binding affinity (Fig. 9). hCNT3 has two Na^+-binding sites, one of which may be Na^+-specific and the other of which may be shared functionally with H^+ (17, 38). hCNT3 Cys-561 seems to be primarily associated with the site interacting with both cations.

In conclusion, two independent lines of investigation have converged to identify Cys-561 as a key residue that resides in a conformationally mobile region of hCNT3 and is intimately involved in both Na^+/nucleoside and H^+/nucleoside cotransport. With actions seemingly specific to one of two hCNT3 cation binding sites, future investigations of Cys-561 and adjacent residues will be central to understanding the molecular intricacies of CNT cation/nucleoside cotransport and, in particular, to functionally separating and structurally identifying the two cation binding domains of hCNT3. Without access to a CNT crystal structure, SCAM-based approaches employing hCNT3C− as a template will be essential to these endeavors.

REFERENCES

1. Cass, C. E. (1995) in *Drug Transport in Antimicrobial and Anticancer Chemotherapy* (Georgopapadakou, N. H., ed) pp. 403–451, Marcel Dekker, New York
2. Griffith, D. A., and Jarvis, S. M. (1996) *Biochim. Biophys. Acta* **1286,** 153–181
3. Young, J. D., Cheeseman, C. I., Mackey, J. R., Cass, C. E., and Baldwin, S. A. (2000) in *Curr. Top. Membr.* **50,** 329–378
4. Damaraju, V. L., Damaraju, S., Young, J. D., Baldwin, S. A., Mackey, J., Sawyer, M. B., and Cass, C. E. (2003) *Oncogene* **22,** 7524–7536
5. Latini, S., and Pedata, F. (2001) *J. Neurochem.* **79,** 463–484
6. King, A. E., Ackley, M. A., Cass, C. E., Young, J. D., and Baldwin, S. A. (2006) *Trends Pharmacol. Sci.* **27,** 416–425
7. Gray, J. H., Owen, R. P., and Giacomini, K. M. (2004) *Pfluegers Arch.* **447,** 728–734
8. Baldwin, S. A., Beal, P. R., Yao, S. Y. M., King, A. E., Cass, C. E., and Young, J. D. (2004) *Pflugers Arch.* **447,** 735–743
9. Elwi, A. N., Damaraju, V. L., Baldwin, S. A., Young, J. D., Sawyer, M. B., and Cass, C. E. (2006) *Biochem. Cell Biol.* **84,** 844–858
10. Damaraju, V. L., Elwi, A. N., Hunter, C., Carpenter, P., Santos, C., Barron, G. M., Sun, X., Baldwin, S. A., Young, J. D., Mackey, J., Sawyer, M. B., and Cass, C. E. (2007) *Am. J. Physiol.* **293,** F200–F211
11. Pastor-Anglada, M., Errasti-Murugarren, E., Aymerich, I., and Casado, F. J. (2007) *J. Physiol. Biochem.* **63,** 97–110
12. Ritzel, M. W. L., Yao, S. Y. M., Huang, M. Y., Elliott, J. F., Cass, C. E., and Young, J. D. (1997) *Am. J. Physiol.* **272,** C707–C714
13. Ritzel, M. W. L., Yao, S. Y. M., Ng, A. M. L., Mackey, J. R., Cass, C. E., and Young, J. D. (1998) *Mol. Membr. Biol.* **15,** 203–211
14. Ritzel, M. W. L., Ng, A. M. L., Yao, S. Y. M., Graham, K., Loewen, S. K., Smith, K. M., Ritzel, R. G., Mowles, D. A., Carpenter, P., Chen, X. -Z., Karpinski, E., Hyde, R. J., Baldwin, S. A., Cass, C. E., and Young, J. D. (2001) *J. Biol. Chem.* **276,** 2914–2927

15. Ritzel, M. W. L., Ng, A. M. L., Yao, S. Y. M., Graham, K., Loewen, S. K., Smith, K. M., Hyde, R. J., Karpinski, E., Cass, C. E., Baldwin, S. A., and Young, J. D. (2001) *Mol. Membr. Biol.* **18,** 65–72
16. Smith, K. M., Ng, A. M. L., Yao, S. Y. M., Labedz, K. A., Knaus, E. E., Wiebe, L. I., Cass, C. E., Baldwin, S. A., Chen, X. -Z., Karpinski, E., and Young, J. D. (2004) *J. Physiol.* **558,** 807–823
17. Smith, K. M., Slugoski, M. D., Loewen, S. K., Ng, A. M. L., Yao, S. Y. M., Chen, X.-Z., Karpinski, E., Cass, C. E., Baldwin, S. A., and Young, J. D. (2005) *J. Biol. Chem.* **280,** 25436–25449
18. Smith, K. M., Slugoski, M. D., Cass, C. E., Baldwin, S. A., Karpinski, E., and Young, J. D. (2007) *Mol. Membr. Biol.* **24,** 53–64
19. Yao, S. Y. M., Ng, A. M. L., Loewen, S. K., Cass, C. E., Baldwin, S. A., and Young, J. D. (2002) *Am. J. Physiol.* **283,** C155–C168
20. Loewen, S. K., Ng, A. M. L., Mohabir, N. N., Baldwin, S. A., Cass, C. E., and Young, J. D. (2003) *Yeast* **20,** 661–675
21. Slugoski, M. D., Loewen, S. K., Ng, A. M. L., Baldwin, S. A., Cass, C. E., and Young, J. D. (2004) *Yeast* **21,** 1269–1277
22. Xiao, G., Wang, J., Tangen, T., and Giacomini, K. M. (2001) *Mol. Pharmacol.* **59,** 339–348
23. Craig, J. E., Zhang, Y., and Gallagher, M. P. (1994) *Mol. Microbiol.* **11,** 1159–1168
24. Loewen, S. K., Yao, S. Y. M., Slugoski, M. D., Mohabir, N. N., Turner, R. J., Mackey, J. R., Weiner, J. H., Gallagher, M. P., Henderson, P. J., Baldwin, S. A., Cass, C. E., and Young, J. D. (2004) *Mol. Membr. Biol.* **21,** 1–10
25. Hamilton, S. R., Yao, S. Y. M., Ingram, J. C., Hadden, D. A., Ritzel, M. W. L., Gallagher, M. P., Henderson, P. J. F., Cass, C. E., Young, J. D., and Baldwin, S. A. (2001) *J. Biol. Chem.* **276,** 27981–27988
26. Loewen, S. K., Ng, A. M. L., Yao, S. Y. M., Cass, C. E., Baldwin, S. A., and Young, J. D. (1999) *J. Biol. Chem.* **274,** 24475–24484
27. Slugoski, M. D., Loewen, S. K., Ng, A. M. L., Smith, K. M., Yao, S. Y. M., Karpinski, E., Cass, C. E., Baldwin, S. A., and Young, J. D. (2007) *Biochemistry* **46,** 1684–1693
28. Yao, S. Y. M., Ng, A. M. L., Slugoski, M. D., Smith, K. M., Mulinta, R., Karpinski, E., Cass, C. E., Baldwin, S. A., and Young, J. D. (2007) *J. Biol. Chem.* **282,** 30607–30617
29. Zhu, Q., and Casey, J. R. (2007) *Methods* **41,** 439–450
30. Kaback, H. R. (2005) *C. R. Biol.* **328,** 557–567
31. Heinze, M., Monden, I., and Keller, K. (2004) *Biochemistry* **43,** 931–936
32. Mueckler, M., and Makepeace, C. (2004) *J. Biol. Chem.* **279,** 10494–10499
33. Fujinaga, J., Tang, X. B., and Casey, J. R. (1999) *J. Biol. Chem.* **274,** 6626–6633
34. Tang, X. B., Kovacs, M., Sterling, D., and Casey, J. R. (1999) *J. Biol. Chem.* **274,** 3557–3564
35. Zhu, Q., Lee, D. W., and Casey, J. R. (2003) *J. Biol. Chem.* **278,** 3112–3120
36. Slepkov, E. R., Rainey, J. K., Li, X., Liu, Y., Cheng, F. J., Lindhout, D. A., Sykes, B. D., and Fliegel, L. (2005) *J. Biol. Chem.* **280,** 17862–17872
37. Zhang, J., Tackaberry, T., Ritzel, M. W., Raborn, T., Barron, G., Baldwin, S. A., Young, J. D., and Cass, C. E. (2006) *Biochem. J.* **394,** 389–398
38. Slugoski, M. D., Ng, A. M. L., Yao, S. Y. M., Smith, K. M., Lin, C. C., Zhang, J., Karpinski, E., Cass, C. E., Baldwin, S. A., and Young, J. D. (2008) *J. Biol. Chem.* **283,** 8496–8507
39. Liman, E. R., Tytgat, J., and Hess, P. (1992) *Neuron* **9,** 861–871
40. Kirsch, R. D., and Joly, E. (1998) *Nucleic Acids Res.* **26,** 1848–1850
41. Yao, S. Y. M., Cass, C. E., and Young, J. D. (2000) in *Membrane Transport: A Practical Approach* (Baldwin, S. A., ed) pp 47–78, Oxford University Press, Oxford
42. Huang, Q. Q., Yao, S. Y. M., Ritzel, M. W., Paterson, A. R., Cass, C. E., and Young, J. D. (1994) *J. Biol. Chem.* **269,** 17757–17760
43. Laemmli, U. K. (1970) *Nature* **227,** 680–685
44. Errasti-Murugarren, E., Cano-Soldado, P., Pastor-Anglada, M., and Casado, F. J. (2008) *Mol. Pharmacol.* **73,** 379–386